Spontaneous Ca²⁺ Fluctuations Arise in Thin Astrocytic Processes With Real 3D Geometry

László Héja[1]*, Zsolt Szabó[1], Márton Péter[1,2] and Julianna Kardos[1]

[1]Functional Pharmacology Research Group, Institute of Organic Chemistry, Research Centre for Natural Sciences, Hungarian Academy of Sciences (MTA), Budapest, Hungary, [2]Hevesy György PhD School of Chemistry, ELTE Eötvös Loránd University, Budapest, Hungary

Fluctuations of cytosolic Ca²⁺ concentration in astrocytes are regarded as a critical non-neuronal signal to regulate neuronal functions. Although such fluctuations can be evoked by neuronal activity, rhythmic astrocytic Ca²⁺ oscillations may also spontaneously arise. Experimental studies hint that these spontaneous astrocytic Ca²⁺ oscillations may lie behind different kinds of emerging neuronal synchronized activities, like epileptogenic bursts or slow-wave rhythms. Despite the potential importance of spontaneous Ca²⁺ oscillations in astrocytes, the mechanism by which they develop is poorly understood. Using simple 3D synapse models and kinetic data of astrocytic Glu transporters (EAATs) and the Na⁺/Ca²⁺ exchanger (NCX), we have previously shown that NCX activity alone can generate markedly stable, spontaneous Ca²⁺ oscillation in the astrocytic leaflet microdomain. Here, we extend that model by incorporating experimentally determined real 3D geometries of 208 excitatory synapses reconstructed from publicly available ultra-resolution electron microscopy datasets. Our simulations predict that the surface/volume ratio (SVR) of peri-synaptic astrocytic processes prominently dictates whether NCX-mediated spontaneous Ca²⁺ oscillations emerge. We also show that increased levels of intracellular astrocytic Na⁺ concentration facilitate the appearance of Ca²⁺ fluctuations. These results further support the principal role of the dynamical reshaping of astrocyte processes in the generation of intrinsic Ca²⁺ oscillations and their spreading over larger astrocytic compartments.

Keywords: astrocyte, Ca²⁺ oscillation, NCX (sodium–calcium exchanger), astrocyte morphology, real geometry, simulation

INTRODUCTION

Over the past three decades, astrocytes have emerged as crucial regulators of synaptic function (Zhang et al., 2016). On the cellular scale, many of these regulatory functions operate by controlling the extracellular concentration of various substances pivotal to synaptic activity (Somogyi et al., 1990; Harris et al., 1992; Rusakov et al., 1997, 1998, 1999; Rusakov and Kullmann, 1998a,b; Araque et al., 1999; Bergles et al., 1999; Ventura and Harris, 1999; Newman, 2004; Matsui et al., 2005; Savtchenko and Rusakov, 2007; Heller et al., 2020). One of such classical astrocyte-mediated regulatory function is the uptake of synaptically released glutamate. Glial glutamate uptake by the Na⁺/Glu symporter, Glu transporters (EAATs), in turn, alters astrocytic intracellular Na⁺ concentration, leading to the activation of diverse Na⁺-symporters, like GABA and Gln transporters or Na⁺/K⁺-ATPase (NKA) and Na⁺/K⁺/2Cl⁻ (NKCC1; Lenart et al., 2004; Héja et al., 2009, 2012, 2019; Pál et al., 2013, 2015; Kirischuk et al., 2016; Gerkau et al., 2019; Henneberger et al., 2020; Lerchundi et al., 2020).

Another consequence of the altered astrocytic Na⁺ concentration is the triggering of coupled Ca^{2+} fluctuations (Mergenthaler et al., 2019) mediated mainly by the Na^+/Ca^{2+} exchanger (NCX; Brazhe et al., 2018). Since NCX operates close to its equilibrium, it can be easily switched between forward and reverse operations (Kirischuk et al., 2016). Moreover, intracellular fluctuations of Na⁺ concentration in the synapse-covering astrocytic microdomain can be intensified by local Na⁺ inhomogeneity due to surface retention of cations by the dipole heads of negatively charged membrane lipids (Breslin et al., 2018). Therefore, EAAT-mediated Glu/Na⁺ symport may easily give rise to local Ca^{2+} fluctuations.

We and others conjectured different Ca^{2+} signaling mechanisms at perisynaptic astrocytic processes (PAPs) and their relevance for the regulation of the tripartite synapses (Kékesi et al., 2015; Kovács et al., 2015; Savtchenko et al., 2015; Kirischuk et al., 2016; Szabó et al., 2017; De Pittà, 2020; Héja and Kardos, 2020; Semyanov et al., 2020). Using a simplified tripartite synapse model built up by geometric modules we have previously shown that NCX alone can generate spontaneous calcium fluctuations, enhanced by glutamate taken up through EAATs (Héja and Kardos, 2020). However, local Na⁺ and Ca^{2+} dynamics in these very thin processes heavily depend on the actual geometry of PAPs. Moreover, this geometry is known to be dynamically changing due to astrocyte activation (Henneberger et al., 2020). Therefore, in the current work, we explored whether NCX activity may introduce rhythmic Ca^{2+} dynamics in real excitatory tripartite synapses using a public annotated database of 1,700 real synapses reconstructed from serial electron microscopic sections (Kasthuri et al., 2015).

MATERIALS AND METHODS

Obtaining Real Geometry of Tripartite Synapses

Real geometry of synapses and surrounding astrocytic processes were obtained from the high-resolution ($6 \times 6 \times 30$ nm) reconstruction of a 1,500 μm^3 volume of mouse neocortex (Kasthuri et al., 2015), containing 1,700 identified and characterized synapses. In the first step, 208 "single" excitatory synapses with individual glutamatergic axon terminal synapsed to single postsynaptic dendritic spines were selected for simulation. Geometry of segmented cells in $1.2 \times 1.2 \times 1.2$ μm volumes ($201 \times 201 \times 41$ pixels) around each post-synaptic density centroid were imported from the database to Matlab using the VAST Lite 1.2.1 software and custom-written Matlab scripts.

To correct geometry for fixation-induced swelling, we shrunk the segmented cells by 6 nm and extended the extracellular space (ECS) to this volume. This way, a fraction of the ECS in the synaptic environment was increased from $11.2 \pm 3.0\%$ to $18.2 \pm 3.3\%$ that is closer to physiological values (Van Harreveld and Khattab, 1968; Harreveld and Fifkova, 1975; Korogod et al., 2015; Pallotto et al., 2015).

Astrocytic coverage of the presynaptic axon terminal (bouton) and the postsynaptic dendritic spine was calculated by counting the number of surface pixels of boutons and spines having close contact with astrocytes. The surface/volume ratio (SVR) was determined by dividing the number of surface pixels counted according to the above method by the number of all pixels belonging to astrocyte processes.

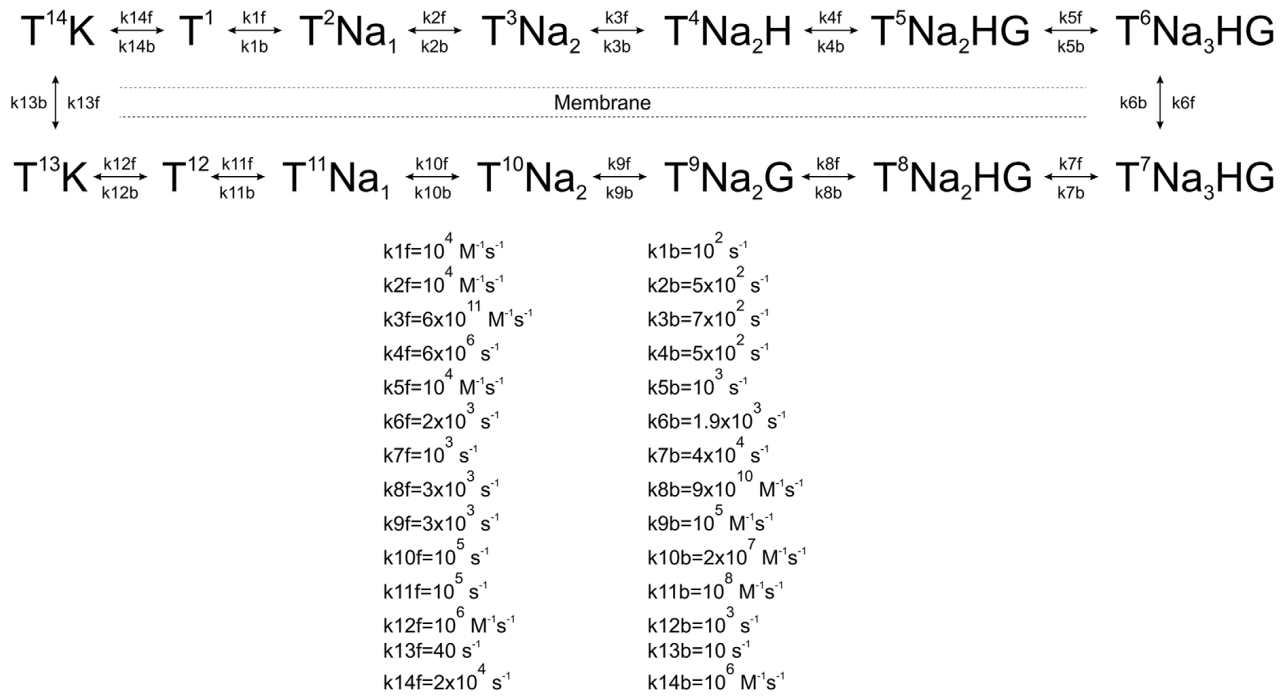## Simulation of Astrocytic [Ca²⁺] and Synaptic Glu Release

Extracellular concentrations of relevant ions ($[Na^+]_e = 140$ mM; $[K^+]_e = 3$ mM; $[Ca^{2+}]_e = 2$ mM) as well as astrocytic $[K^+]_i$ (130 mM) and $[Glu]_i$ (3 mM) were kept constant during the simulation, while $[Glu]_e$ (0.3 μM), $[Na^+]_i$ (15 mM) and $[Ca^{2+}]_i$ (100 nM) were allowed to change due to Glu release, intracellular Ca^{2+} diffusion and activation of EAATs and NCX (Héja and Kardos, 2020). It is to note that $[Glu]_e$ is difficult to measure and rather different estimates are reported in the literature. Electrophysiological measurements suggest tens of nanomolar concentrations (Herman et al., 2011) based on receptor activation, while microdialysis studies measure tens of micromolar for $[Glu]_e$ (Baker et al., 2002). Furthermore, EC_{50} values of postsynaptic glutamate receptor (382 μM; Jonas and Sakmann, 1992; Li et al., 2002) and astrocytic glutamate transporter (14.8 μM; Levy et al., 1998; Herman and Jahr, 2007) indicate effective activation of postsynaptic receptors and extrasynaptic transporters at above 100 μM and 3 μM glutamate, respectively. These glutamate concentration ranges are far beyond the $[Glu]_e$ of 0.4 ± 0.1 μM (Kékesi et al., 2000) allowing for receptor/transporter activation. Our in vivo microdialysis data also validates the mean of these values as being 0.4 ± 0.1 μM (Kékesi et al., 2000). Therefore, 0.3 μM $[Glu]_e$, used in this study seems a reliable estimate.

Markovian kinetic models of astrocytic EAATs and NCX were constructed according to published rate constants based on experimental data. Glutamate uptake by EAATs was modeled by a 13-step cycle comprised of separate bindings and unbindings of 3 Na⁺, 1H⁺, 1 K⁺, and 1 Glu molecules (Bergles et al., 2002). NCX activity was modeled by a 6-step cycle according to Chu et al. (2016). $10,800/\mu m^2$ EAAT (Lehre and Danbolt, 1998) and $500/\mu m^2$ NCX (Chu et al., 2016) molecules were distributed randomly on the astrocytic surface.

Before starting the simulation, EAAT and NCX randomly populated the available states and we allowed them to reach steady-state distribution for 30 ms at the above concentrations. Simulations began with a further 10 ms baseline activity before initiating single synaptic glutamate release (5,000 Glu molecules) at the synapse centroid as determined by Kasthuri et al. (2015). The diffusion of independent glutamate molecules in the 3D ECS was estimated by random walks at 1 μs intervals. The diffusion coefficient of glutamate was set to 0.33 $\mu m^2/ms$ (Gavrilov et al., 2018).

Each time steps (1 μs) was comprised of the following functions: (1) position of extracellular glutamate molecules and intracellular Ca^{2+} ions were updated by moving them with normally distributed random distances around their mean square displacement values. If a particle moved outside of the sample volume, it was removed from the available pool, except if $[Glu]_e$, $[Na^+]_i$ or $[Ca^{2+}]_i$ dropped below the baseline level, in

EAAT

$$T^{14}K \underset{k14b}{\overset{k14f}{\rightleftharpoons}} T^1 \underset{k1b}{\overset{k1f}{\rightleftharpoons}} T^2Na_1 \underset{k2b}{\overset{k2f}{\rightleftharpoons}} T^3Na_2 \underset{k3b}{\overset{k3f}{\rightleftharpoons}} T^4Na_2H \underset{k4b}{\overset{k4f}{\rightleftharpoons}} T^5Na_2HG \underset{k5b}{\overset{k5f}{\rightleftharpoons}} T^6Na_3HG$$

k13b | k13f .... Membrane .... k6b | k6f

$$T^{13}K \underset{k12b}{\overset{k12f}{\rightleftharpoons}} T^{12} \underset{k11b}{\overset{k11f}{\rightleftharpoons}} T^{11}Na_1 \underset{k10b}{\overset{k10f}{\rightleftharpoons}} T^{10}Na_2 \underset{k9b}{\overset{k9f}{\rightleftharpoons}} T^9Na_2G \underset{k8b}{\overset{k8f}{\rightleftharpoons}} T^8Na_2HG \underset{k7b}{\overset{k7f}{\rightleftharpoons}} T^7Na_3HG$$

k1f=10^4 M^{-1}s^{-1}

k2f=10^4 M^{-1}s^{-1}

k3f=6×10^{11} M^{-1}s^{-1}

k4f=6×10^6 s^{-1}

k5f=10^4 M^{-1}s^{-1}

k6f=2×10^3 s^{-1}

k7f=10^3 s^{-1}

k8f=3×10^3 s^{-1}

k9f=3×10^3 s^{-1}

k10f=10^5 s^{-1}

k11f=10^5 s^{-1}

k12f=10^6 M^{-1}s^{-1}

k13f=40 s^{-1}

k14f=2×10^4 s^{-1}

k1b=10^2 s^{-1}

k2b=5×10^2 s^{-1}

k3b=7×10^2 s^{-1}

k4b=5×10^2 s^{-1}

k5b=10^3 s^{-1}

k6b=1.9×10^3 s^{-1}

k7b=4×10^4 s^{-1}

k8b=9×10^{10} M^{-1}s^{-1}

k9b=10^5 M^{-1}s^{-1}

k10b=2×10^7 M^{-1}s^{-1}

k11b=10^8 M^{-1}s^{-1}

k12b=10^3 s^{-1}

k13b=10 s^{-1}

k14b=10^6 M^{-1}s^{-1}

NCX

$$T^6Ca \underset{k6b}{\overset{k6f}{\rightleftharpoons}} T^1 \underset{k1b}{\overset{k1f}{\rightleftharpoons}} T^2Na$$

k5b | k5f .... Membrane .... k2b | k2f

$$T^5Ca \underset{k4b}{\overset{k4f}{\rightleftharpoons}} T^4 \underset{k3b}{\overset{k3f}{\rightleftharpoons}} T^3Na$$

k1f=4.325×10^{10} M^{-3}s^{-1}

k2f=1.0781×10^4 s^{-1}

k3f=1.408×10^4 s^{-1}

k4f=4.024×10^8 s^{-1}

k5f=7.1389×10^3 s^{-1}

k6f=4.5134×10^3 s^{-1}

k1b=1.0524×10^4 s^{-1}

k2b=3.3541×10^3 s^{-1}

k3b=2.8692×10^9 s^{-1}

k4b=7.3916×10^3 s^{-1}

k5b=9.4959×10^3 s^{-1}
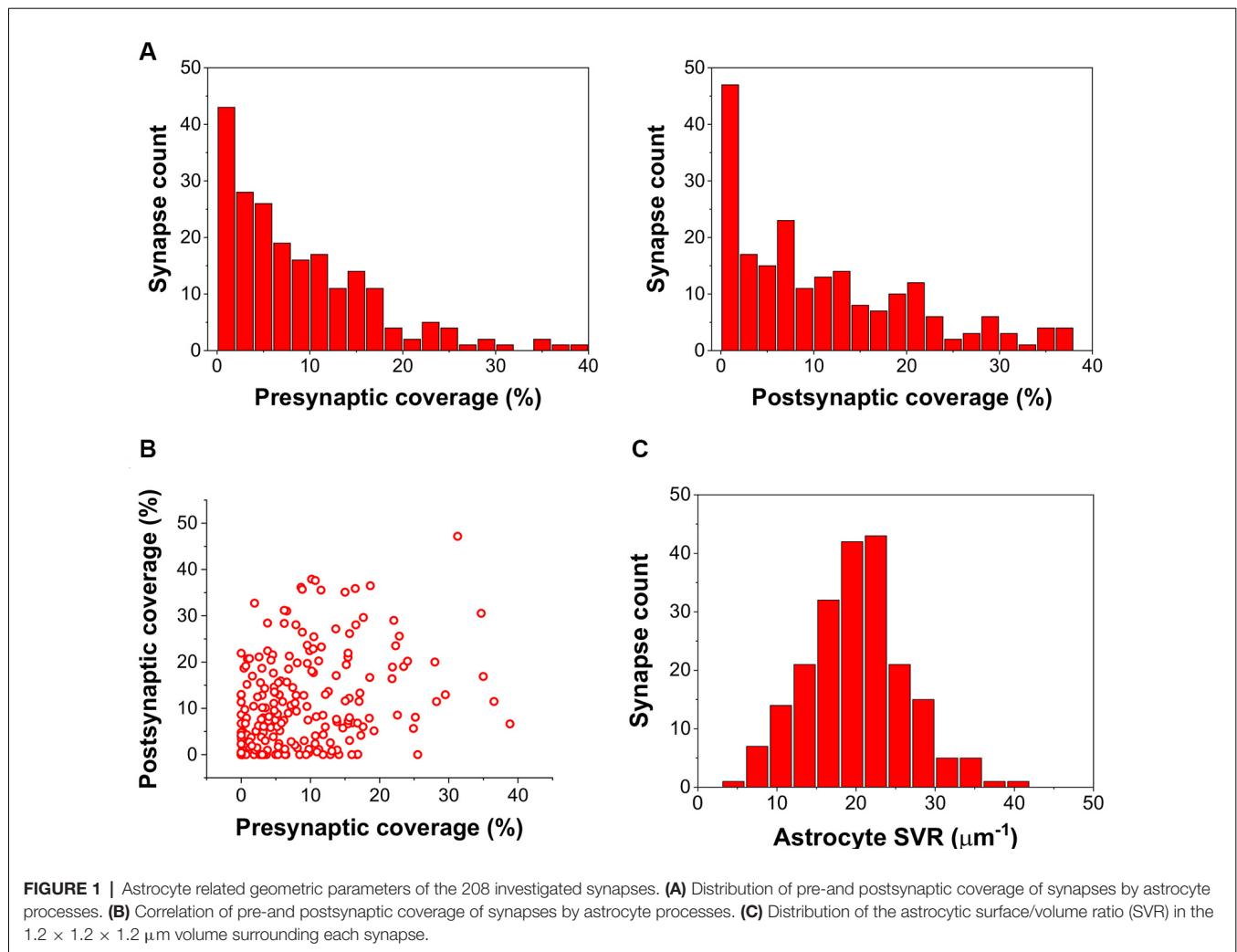
k6b=1.0691×10^{10} M^{-1}s^{-1}

SCHEME 1 | Kinetic schemes and rates of astrocytic Glu transporters (EAAT) and Na$^+$/Ca^{2+} exchanger (NCX).

which case it was moved back to its previous position. Particles moving out of their compartment (astrocyte, dendrite, axon terminal, or ECS) were also placed back to their previous position. (2) Transition states of EAAT and NCX molecules were determined according to their rate constants and dynamic rate constants based on the current intra- and extracellular concentrations of relevant ions (**Scheme 1**). In the case of EAAT kinetics, local [Glu]$_e$ in the surrounding $50 \times 50 \times 50$ nm^3 extracellular microdomain of each EAAT molecule was used instead of the average extracellular glutamate concentration.

Local [Glu]$_e$ was determined by counting the freely diffusing Glu molecules in the $50 \times 50 \times 50$ nm^3 ECS around each EAATs in each time frame. Transition rates were corrected for $Q_{10} = 3$ to account for temperature dependence. Astrocyte membrane potential was set to -70 mV. (3) Glutamate molecules bound to the extracellularly faced EAAT were removed from the available pool until they were released back by reverse operation of the transporter. Ca^{2+} ions bound to the intracellularly faced NCX were removed from the available pool until they were released back by reverse operation of the transporter.

FIGURE 1 | Astrocyte related geometric parameters of the 208 investigated synapses. **(A)** Distribution of pre-and postsynaptic coverage of synapses by astrocyte processes. **(B)** Correlation of pre-and postsynaptic coverage of synapses by astrocyte processes. **(C)** Distribution of the astrocytic surface/volume ratio (SVR) in the 1.2 × 1.2 × 1.2 μm volume surrounding each synapse.

All simulations were done in Matlab using custom-written scripts[1]. Reconstructed and segmented EM stacks of real synapses were downloaded and handled by the VAST Lite 1.2.1 software[2] (Kasthuri et al., 2015) and the VastTools Matlab package. Processed data of synapses containing 3D geometries and calculated surfaces and volumes in Matlab file format as well as tools to reproduce the simulations can be downloaded at http://downloadables.ttk.hu/heja/Front_CellNeurosci2021. Synapses were visualized using Cinema4D.

Data are shown as mean ± SEM and were analyzed with one-way analysis of variances (ANOVAs, OriginPro 2018). Statistical significance was considered at $p < 0.05$.

RESULTS

To simulate Ca²⁺ oscillations in real astrocyte processes, we used the saturated reconstruction of a 1,500 μm³ volume of mouse neocortex (Kasthuri et al., 2015). The dataset contains

1,700 identified and morphologically characterized synapses. We explored volumes of 1.2 × 1.2 × 1.2 μm around these synapses to investigate the potential of astrocytic processes to readout synaptic activity.
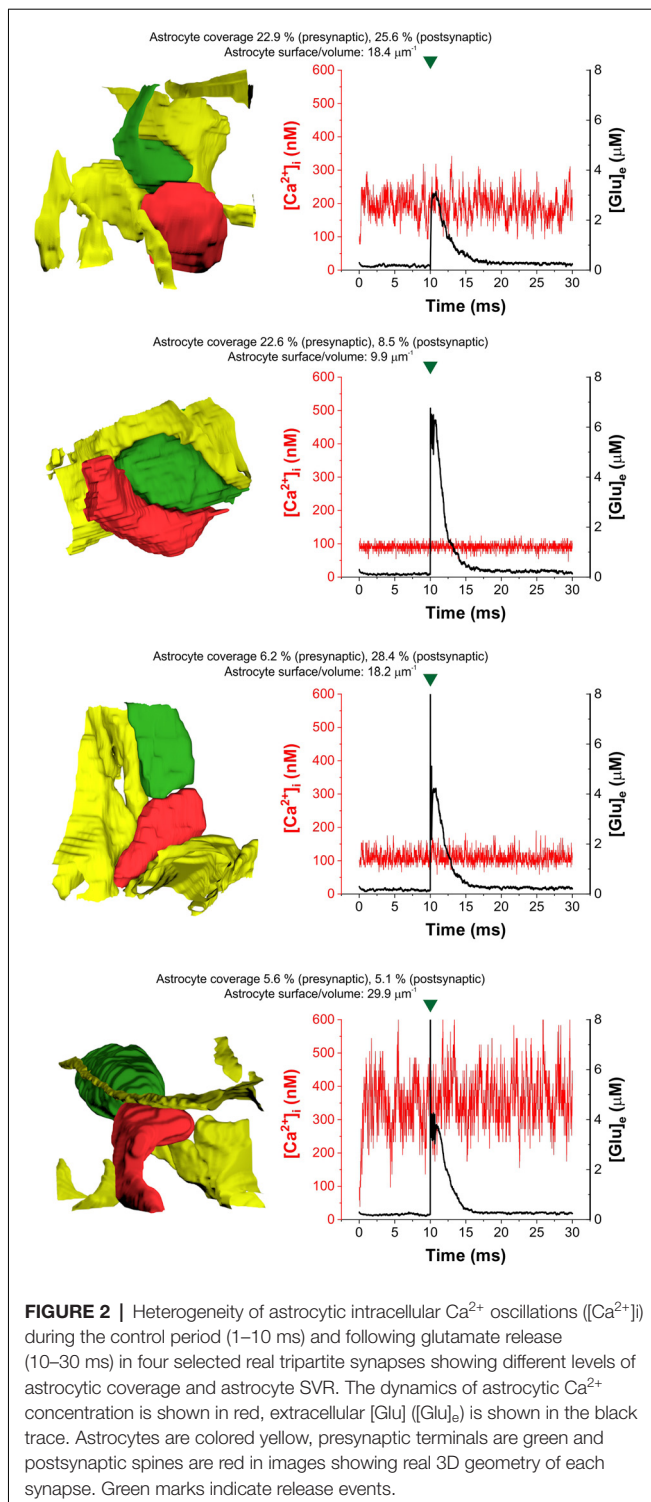
Due to the applied glutaraldehyde and paraformaldehyde fixative, the ECS of the sample was found to occupy only 6% of the total volume around the synapses (Kasthuri et al., 2015). Since ECS fraction was found to be between 15% and 25% in frozen tissues (Van Harreveld and Khattab, 1968; Harreveld and Fifkova, 1975; Korogod et al., 2015; Pallotto et al., 2015) where fixation-issued swelling is not present, we modified the original segmentation by replacing the outer 6 nm surface of each cellular segment with ECS. This modification also allowed free diffusion of the released glutamate in the ECS, which would otherwise be hindered due to the direct connection of segmented cells.

To simulate spontaneous and glutamate-release associated, NCX activity-linked Ca²⁺ changes in real glutamatergic tripartite synapses, we selected 208 "classical" synapses out of the 1,700 identified synapses (Kasthuri et al., 2015) based on the following criteria: (1) axon type is excitatory; (2) axon terminal is present, i.e., it is not an en-passant synapse; (3) axon bouton
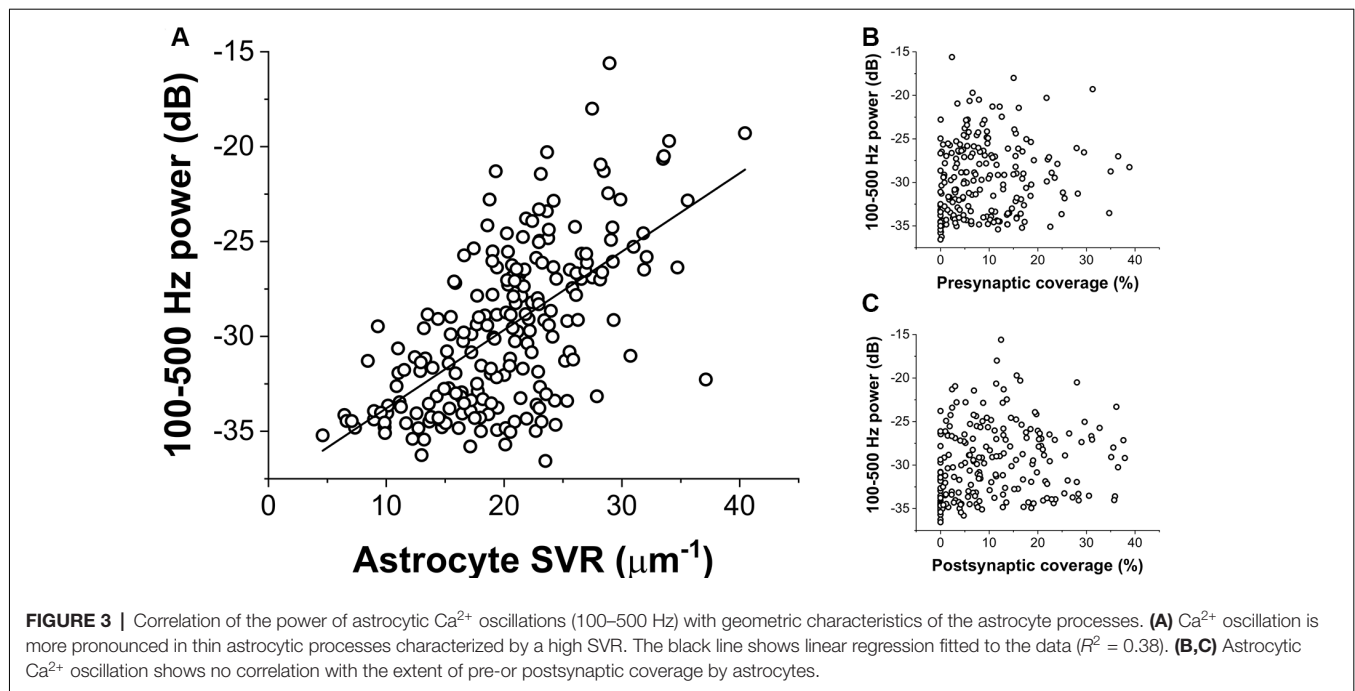
---

[1]https://github.com/hejalaszlo/Astrocyte-leaflet-simulation
[2]https://lichtman.rc.fas.harvard.edu/vast/

FIGURE 2 | Heterogeneity of astrocytic intracellular Ca²⁺ oscillations ([Ca²⁺]i) during the control period (1–10 ms) and following glutamate release (10–30 ms) in four selected real tripartite synapses showing different levels of astrocytic coverage and astrocyte SVR. The dynamics of astrocytic Ca²⁺ concentration is shown in red, extracellular [Glu] ([Glu]ₑ) is shown in the black trace. Astrocytes are colored yellow, presynaptic terminals are green and postsynaptic spines are red in images showing real 3D geometry of each synapse. Green marks indicate release events.

is not multi-synaptic; (4) the postsynaptic element is a spine, not a shaft; and (5) astrocytic volume fraction is at least 2% in the 1.2 × 1.2 × 1.2 µm volume. Astrocytic Ca²⁺, extracellular glutamate concentrations following synaptic Glu release, as well as dynamics of astrocytic Glu transporters (EAAT) and NCX were simulated as previously described (Héja and Kardos, 2020).

By calculating the ratio of the axon terminal and spine surfaces that are in contact with astrocytic processes, we found many presynaptic axon terminals and postsynaptic spines with little or no astrocytic coverage at all (**Figure 1A**). Also, astrocytic coverage of pre- and postsynaptic elements showed a high degree of heterogeneity (**Figure 1B**). Although many of the synapses were equally covered by astrocytes at the axon terminal and the dendritic spine, highly asymmetric astrocytic coverage was also abundant. Besides, we also determined the surface to volume ratio (SVR) of astrocytic processes in the surrounding of the 208 selected synapses. Following previous observations (Gavrilov et al., 2018), the distribution of SVR followed normal distributions with a mean between 20 and 25 µm⁻¹, corresponding to astrocytic leaflets that are known to cover synapses (Gavrilov et al., 2018; **Figure 1C**).

In agreement with previous findings (Héja and Kardos, 2020), we found that astrocytic oscillatory Ca²⁺ dynamics spontaneously emerged in different kinds of realistic astrocytic leaflets characterized by various pre- or postsynaptic contacts (**Figure 2**). The incidence of Ca²⁺ fluctuations strongly depends on the astrocytic SVR and also correlates with pre- and postsynaptic astrocytic coverage (**Figure 2**). High astrocytic SVR frequently correlated with large amplitude fluctuations of astrocytic Ca²⁺ concentration both spontaneously and following glutamate release (**Figure 2**). Medium SVR in conjunction with high coverage of both presynaptic axon terminal and postsynaptic dendritic spine is characterized by the medium intensity of Ca²⁺ fluctuations that is unaffected by glutamate release (**Figure 2**). On the other hand, no astrocytic Ca²⁺ fluctuations emerge at low SVR (**Figure 2**).

To quantify the extent of NCX-mediated astrocytic Ca²⁺ oscillations, we calculated the power spectral density of the Ca²⁺ signal and summed its power in a wide range between 100 and 500 Hz. The power of these high-frequency Ca²⁺ oscillations showed a direct correlation with increasing SVR, i.e., it is more apparent in thin astrocytic processes (**Figure 3A**). By contrast, the power of high-frequency Ca²⁺ fluctuations does not depend on either pre- or postsynaptic astrocytic coverage (**Figures 3B,C**).

Furthermore, we also investigated whether synaptic glutamate release alters the spontaneous NCX-mediated Ca²⁺ fluctuations. To this end, we compared the oscillatory powers of the Ca²⁺ concentration signals in the 100–500 Hz range in two different conditions: (1) simulating baseline Ca²⁺ fluctuations when only NCX was allowed to operate and no synaptic glutamate release occurred; and (2) simulating Ca²⁺ fluctuations according to our original conditions, releasing 5,000 glutamate molecule after 10 ms of baseline activity and letting EAATs function. The powers of the 100–500 Hz range of the Ca²⁺ concentration signals were compared in the 12–21 ms period. In some synapses, glutamate release significantly increased the 100–500 Hz power. As an example, 100–500 Hz power increased from −23.85 ± 0.20 dB to −22.72 ± 0.27 dB due to synaptic glutamate release ($n = 5$ simulation runs, $p = 0.01$) in a synapse with high SVR (22.4 µm⁻¹; **Figure 4A**). However, although a slight increase was also observed on the population
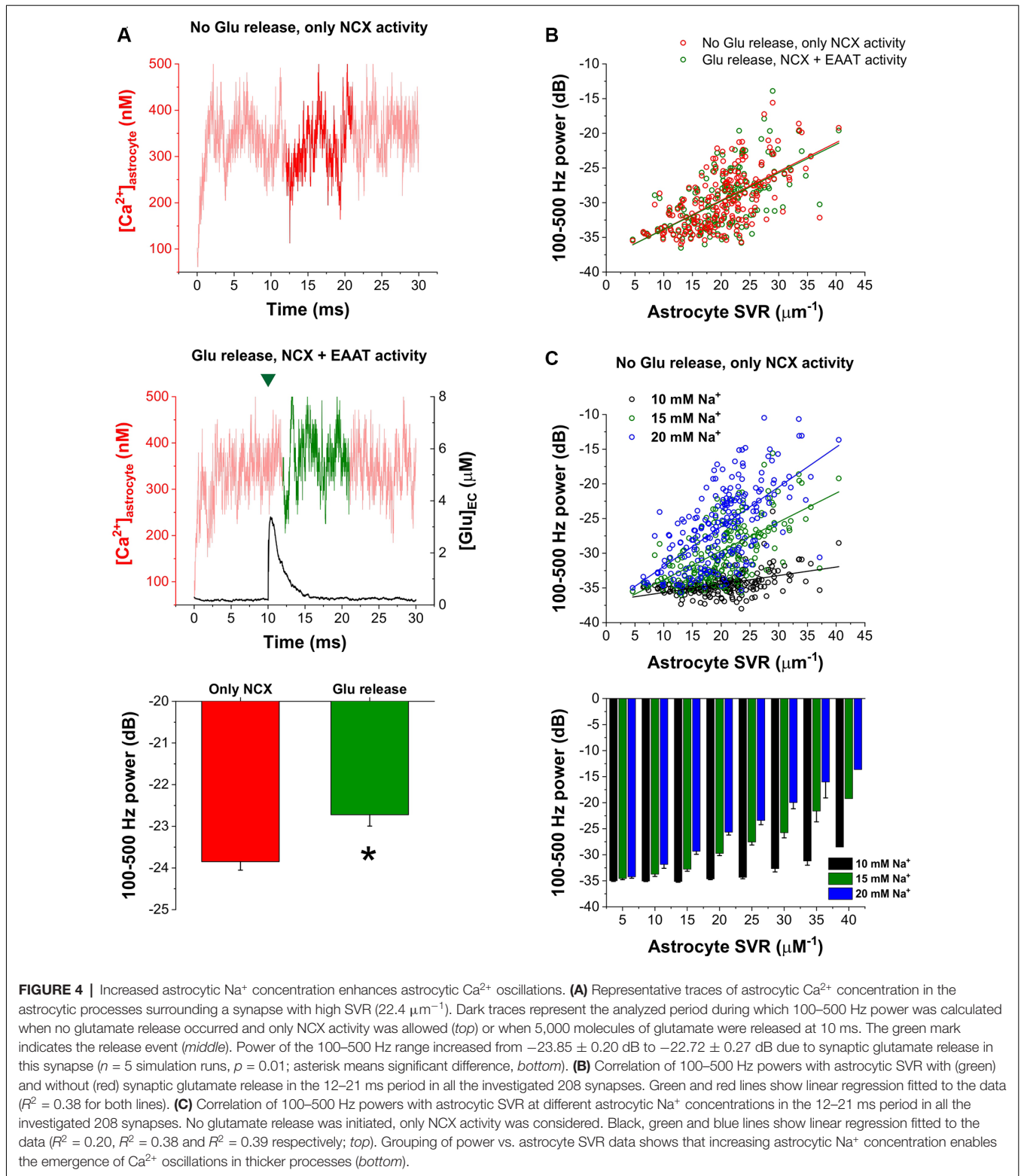
FIGURE 3 | Correlation of the power of astrocytic Ca²⁺ oscillations (100–500 Hz) with geometric characteristics of the astrocyte processes. **(A)** Ca²⁺ oscillation is more pronounced in thin astrocytic processes characterized by a high SVR. The black line shows linear regression fitted to the data (R^2 = 0.38). **(B,C)** Astrocytic Ca²⁺ oscillation shows no correlation with the extent of pre-or postsynaptic coverage by astrocytes.

level, this increase was not significant (-29.73 ± 0.29 dB vs. -29.61 ± 0.29 dB, n = 208 synapses, p = 0.09). Therefore, we investigated whether synapses characterized by different SVR of the surrounding astrocytes may respond differently to Glu release. Resolution of Glu release-induced changes in the power of astrocytic Ca²⁺ fluctuations by astrocyte SVRs, however, still did not reveal a significant effect of Glu release (**Figure 4B**). Since single Glu release events only slightly increase astrocytic Na⁺ concentration, we investigated whether more pronounced (but still physiological) changes in astrocytic Na⁺ concentration may significantly affect NCX-mediated Ca²⁺ fluctuations. Changing astrocytic Na⁺ concentration from the original 15 mM to 10 or 20 mM, indeed, markedly altered Ca²⁺ oscillatory power (**Figure 4C**). Increasing astrocytic Na⁺ concentration enhances Ca²⁺ fluctuations in general, and consequently allows the emergence of such oscillations in thicker processes characterized by smaller SVR.

DISCUSSION

Spontaneous astroglial Ca²⁺ fluctuations, mediated by NCX in real excitatory tripartite synapses appear to be primarily dependent on astrocytic SVR. In our simulations, more pronounced NCX-operated Ca²⁺ fluctuations are associated with high SVR, suggesting that thin astrocytic processes are capable to spontaneously generate astrocytic Ca²⁺ signals. Although, we found that NCX mediated spontaneous Ca²⁺ fluctuations are not significantly modulated by single Glu release events and corresponding Na⁺ entry through plasma membrane glutamate transporters, we showed that increasing astrocytic Na⁺ concentration in the physiological range markedly enhances Ca²⁺ fluctuations in real tripartite synapses, especially in those, characterized by high SVR. Therefore, we hypothesize

that bursting synaptic activity or simultaneous activation of multiple synapses in the domain of a single astrocyte may significantly contribute to the emergence and enhancement of Ca²⁺ fluctuations by increasing astrocytic Na⁺ concentration. The scenario with Na⁺ threshold and mechanistic explanation, however, remains to be clarified. Importantly, astrocytic Ca²⁺ concentration can also be directly increased by the activation of astrocytic NMDA receptors (Ziemens et al., 2019) that are currently not included in our model.

It is evident from our simulations that the appearance of fast Ca²⁺ fluctuations is correlated to the high surface-to-volume ratio of PAPs. Unfortunately, neither spatial nor temporal resolution of current experimental techniques allows the direct observation of such fast (>100 Hz) Ca²⁺ signals in tiny processes (d < 2–300 nm, SVR > 10; Rusakov, 2015). Therefore, we can only speculate about how these spontaneous Ca²⁺ events, triggered by Ca²⁺ entry through NCX can propagate into astrocytic branchlets and can be amplified and propagated as a result of various downstream mechanisms, including Ca²⁺-dependent Ca²⁺ release in association with activation of inositol 1,4,5-trisphosphate receptors (IP₃R) or mitochondrial permeability transition pores (Semyanov et al., 2020). It was experimentally observed, however, that the appearance and frequency of slower spontaneous Ca²⁺ events in somewhat larger astrocytic processes (characterized by SVR < 3) depend on SVR (Wu et al., 2019). Also, compartmentalized Ca²⁺ waves as predicted by the dynamically rich repertoire of distinct Ca²⁺-dependent Ca²⁺ release dynamics (Matrosov et al., 2019) may travel and act by modulating local spontaneous Ca²⁺ fluctuations. Indeed, the shape of the slow Ca²⁺ wave with fast Ca²⁺ fluctuations (Savtchenko et al., 2018; SI Figure 12) may indicate the superimposition of slow waves and fast Ca²⁺ fluctuations locally. It is to mention, that fast astrocytic Ca²⁺

FIGURE 4 | Increased astrocytic Na^+ concentration enhances astrocytic Ca^{2+} oscillations. **(A)** Representative traces of astrocytic Ca^{2+} concentration in the astrocytic processes surrounding a synapse with high SVR (22.4 μm^{-1}). Dark traces represent the analyzed period during which 100–500 Hz power was calculated when no glutamate release occurred and only NCX activity was allowed (*top*) or when 5,000 molecules of glutamate were released at 10 ms. The green mark indicates the release event (*middle*). Power of the 100–500 Hz range increased from -23.85 ± 0.20 dB to -22.72 ± 0.27 dB due to synaptic glutamate release in this synapse ($n = 5$ simulation runs, $p = 0.01$; asterisk means significant difference, *bottom*). **(B)** Correlation of 100–500 Hz powers with astrocytic SVR with (green) and without (red) synaptic glutamate release in the 12–21 ms period in all the investigated 208 synapses. Green and red lines show linear regression fitted to the data ($R^2 = 0.38$ for both lines). **(C)** Correlation of 100–500 Hz powers with astrocytic SVR at different astrocytic Na^+ concentrations in the 12–21 ms period in all the investigated 208 synapses. No glutamate release was initiated, only NCX activity was considered. Black, green and blue lines show linear regression fitted to the data ($R^2 = 0.20$, $R^2 = 0.38$ and $R^2 = 0.39$ respectively; *top*). Grouping of power vs. astrocyte SVR data shows that increasing astrocytic Na^+ concentration enables the emergence of Ca^{2+} oscillations in thicker processes (*bottom*).

signaling with mean onset time as rapid as that of neurons is not unprecedented (Kékesi et al., 2015; Pál et al., 2015; Lind et al., 2018; Stobart et al., 2018; Semyanov et al., 2020). Assessing the true impact of spontaneously emerging, local high-frequency Ca^{2+} fluctuations on the evolution of cellular- and network-scale Ca^{2+} oscillations necessitates further studies, that include models describing downstream Ca^{2+} stores and Ca^{2+} buffers (Savtchenko et al., 2018; Matrosov et al., 2019), as well as simulate

Ca^{2+} dynamics in multiple, neighboring synapses contacted by the same astrocyte. We may also conjecture that the structural plasticity of astrocytic processes may serve as a *de novo* signal generator, independently of its role in regulating glutamate spillover, K^{+} buffering, or other indirect forms of modulation of neuronal activity (Henneberger et al., 2020). These findings suggest a prominent role for dynamically changing PAPs in neuro-glial coupling.

DATA AVAILABILITY STATEMENT

Raw data is available to download at http://downloadables.ttk.hu/heja/Front_Cell_Neurosci_2021. Matlab scripts used to process the data can be downloaded at https://github.com/hejalaszlo/Astrocyte-leaflet-simulation.

AUTHOR CONTRIBUTIONS

LH: conceptualization, data curation, formal analysis, funding acquisition, methodology, software, supervision, validation, visualization, roles/writing—original draft, writing—review and editing. ZS and MP: data curation, methodology, validation, roles/writing—original draft, writing—review and editing. JK: conceptualization, investigation, methodology, supervision, roles/writing—original draft, writing—review and editing. All authors contributed to the article and approved the submitted version.

FUNDING

ACKNOWLEDGMENTS

REFERENCES

Araque, A., Parpura, V., Sanzgiri, R. P., and Haydon, P. G. (1999). Tripartite synapses: glia, the unacknowledged partner. *Trends Neurosci.* 22, 208–215. doi: 10.1016/s0166-2236(98)01349-6

Baker, D. A., Shen, H., and Kalivas, P. W. (2002). Cystine/glutamate exchange serves as the source for extracellular glutamate: modifications by repeated cocaine administration. *Amino Acids* 23, 161–162. doi: 10.1007/s00726-001-0122-6

Bergles, D. E., Diamond, J. S., and Jahr, C. E. (1999). Clearance of glutamate inside the synapse and beyond. *Curr. Opin. Neurobiol.* 9, 293–298. doi: 10.1016/s0959-4388(99)80043-9

Bergles, D. E., Tzingounis, A. V., and Jahr, C. E. (2002). Comparison of coupled and uncoupled currents during glutamate uptake by GLT-1 transporters. *J. Neurosci.* 22, 10153–10162. doi: 10.1523/JNEUROSCI.22-23-10153.2002

Brazhe, A. R., Verisokin, A. Y., Verveyko, D. V., and Postnov, D. E. (2018). Sodium-calcium exchanger can account for regenerative Ca^{2+} entry in thin astrocyte processes. *Front. Cell. Neurosci.* 12:250. doi: 10.3389/fncel.2018.00250

Breslin, K., Wade, J. J., Wong-Lin, K., Harkin, J., Flanagan, B., Van Zalinge, H., et al. (2018). Potassium and sodium microdomains in thin astroglial processes: A computational model study. *PLoS Comput. Biol.* 14:e1006151. doi: 10.1371/journal.pcbi.1006151

Chu, L., Greenstein, J. L., and Winslow, R. L. (2016). Modeling Na^{+}-Ca^{2+} exchange in the heart: allosteric activation, spatial localization, sparks and excitation-contraction coupling. *J. Mol. Cell. Cardiol.* 99, 174–187. doi: 10.1016/j.yjmcc.2016.06.068

De Pittà, M. (2020). "Neuron-glial interactions," in *Encyclopedia of Computational Neuroscience*. New York, NY: Springer New York, 1–30.

Gavrilov, N., Golyagina, I., Brazhe, A., Scimemi, A., Turlapov, V., and Semyanov, A. (2018). Astrocytic coverage of dendritic spines, dendritic shafts and axonal boutons in hippocampal neuropil. *Front. Cell. Neurosci.* 12:248. doi: 10.3389/fncel.2018.00248

Gerkau, N. J., Lerchundi, R., Nelson, J. S. E., Lantermann, M., Meyer, J., Hirrlinger, J., et al. (2019). Relation between activity-induced intracellular sodium transients and ATP dynamics in mouse hippocampal neurons. *J. Physiol.* 597, 5687–5705. doi: 10.1113/JP278658

Harris, K. M., Jensen, F. E., and Tsao, B. (1992). Three-dimensional structure of dendritic spines and synapses in rat hippocampus (CA1) at postnatal day 15 and adult ages: Implications for the maturation of synaptic physiology and long-term potentiation. *J. Neurosci.* 12, 2685–2705. doi: 10.1523/JNEUROSCI.12-07-02685.1992

Héja, L., Barabás, P., Nyitrai, G., Kékesi, K. A. K. A., Lasztóczi, B., Toke, O., et al. (2009). Glutamate uptake triggers transporter-mediated GABA release from astrocytes. *PLoS One* 4:e7153. doi: 10.1371/journal.pone.0007153

Héja, L., and Kardos, J. (2020). NCX activity generates spontaneous Ca^{2+} oscillations in the astrocytic leaflet microdomain. *Cell Calcium* 86:102137. doi: 10.1016/j.ceca.2019.102137

Héja, L., Nyitrai, G., Kékesi, O., and Dobolyi, Á. (2012). Astrocytes convert network excitation to tonic inhibition of neurons. *BMC Biol.* 10:26. doi: 10.1186/1741-7007-10-26

Héja, L., Simon, Á., Szabó, Z., and Kardos, J. (2019). Feedback adaptation of synaptic excitability *via* Glu:Na^{+} symport driven astrocytic GABA and Gln release. *Neuropharmacology* 161:107629. doi: 10.1016/j.neuropharm.2019.05.006

Heller, J. P., Odii, T., Zheng, K., and Rusakov, D. A. (2020). Imaging tripartite synapses using super-resolution microscopy. *Methods* 174, 81–90. doi: 10.1016/j.ymeth.2019.05.024

Henneberger, C., Bard, L., Panatier, A., Reynolds, J. P., Kopach, O., Medvedev, N. I., et al. (2020). LTP induction boosts glutamate spillover by driving withdrawal of perisynaptic astroglia. *Neuron* 108, e11919–e11936. doi: 10.1016/j.neuron.2020.08.030

Herman, M. A., and Jahr, C. E. (2007). Extracellular glutamate concentration in hippocampal slice. *J. Neurosci.* 27, 9736–9741. doi: 10.1523/JNEUROSCI.3009-07.2007

Herman, M. A., Nahir, B., and Jahr, C. E. (2011). Distribution of extracellular glutamate in the neuropil of hippocampus. *PLoS One* 6:e26501. doi: 10.1371/journal.pone.0026501

Jonas, P., and Sakmann, B. (1992). Glutamate receptor channels in isolated patches from CA1 and CA3 pyramidal cells of rat hippocampal slices. *J. Physiol.* 455, 143–171. doi: 10.1113/jphysiol.1992.sp019294

Kasthuri, N., Hayworth, K. J., Berger, D. R., Schalek, R. L., Conchello, J. A., Knowles-Barley, S., et al. (2015). Saturated reconstruction of a volume of neocortex. *Cell* 162, 648–661. doi: 10.1016/j.cell.2015.06.054

Kékesi, O., Ioja, E. E., Szabó, Z., Kardos, J., and Héja, L. (2015). Recurrent seizure-like events are associated with coupled astroglial synchronization. *Front. Cell. Neurosci.* 9:215. doi: 10.3389/fncel.2015.00215

Kékesi, K. A., Szilágyi, N., Nyitrai, G., Árpád, D., Skuban, N., and Kardos, J. (2000). Persistent depolarization and Glu uptake inhibition operate distinct

osmoregulatory mechanisms in the mammalian brain. *Neurochem. Int.* 37, 171–178. doi: 10.1016/s0197-0186(00)00020-6

Kirischuk, S., Héja, L., Kardos, J., and Billups, B. (2016). Astrocyte sodium signaling and the regulation of neurotransmission. *Glia.* 64, 1655–1666. doi: 10.1002/glia.22943

Korogod, N., Petersen, C. C. H., and Knott, G. W. (2015). Ultrastructural analysis of adult mouse neocortex comparing aldehyde perfusion with cryo fixation. *eLife* 4:e05793. doi: 10.7554/eLife.05793

Kovács, Z., Kékesi, K. A., Juhász, G., Barna, J., Héja, L., Lakatos, R., et al. (2015). Non-adenosine nucleoside inosine, guanosine and uridine as promising antiepileptic drugs: a summary of current literature. *Mini Rev. Med. Chem.* 14, 1033–1042. doi: 10.2174/1389557514666141107120226

Lehre, K. P., and Danbolt, N. C. (1998). The number of glutamate transporter subtype molecules at glutamatergic synapses: chemical and stereological quantification in young adult rat brain. *J. Neurosci.* 18, 8751–8757. doi: 10.1523/JNEUROSCI.18-21-08751.1998

Lenart, B., Kintner, D. B., Shull, G. E., and Sun, D. (2004). Na-K-Cl cotransporter-mediated intracellular Na$^+$ accumulation affects Ca^{2+} signaling in astrocytes in an in vitro ischemic model. *J. Neurosci.* 24, 9585–9597. doi: 10.1523/JNEUROSCI.2569-04.2004

Lerchundi, R., Huang, N., and Rose, C. R. (2020). Quantitative imaging of changes in astrocytic and neuronal adenosine triphosphate using two different variants of ATeam. *Front. Cell. Neurosci.* 14:80. doi: 10.3389/fncel.2020.00080

Levy, L. M., Warr, O., and Attwell, D. (1998). Stoichiometry of the glial glutamate transporter GLT-1 expressed inducibly in a Chinese hamster ovary cell line selected for low endogenous Na$^+$-dependent glutamate uptake. *J. Neurosci.* 18, 9620–9628. doi: 10.1523/JNEUROSCI.18-23-09620.1998

Li, H., Nowak, L. M., Gee, K. R., and Hess, G. P. (2002). Mechanism of glutamate receptor-channel function in rat hippocampal neurons investigated using the laser-pulse photolysis (LaPP) technique. *Biochemistry* 41, 4753–4759. doi: 10.1021/bi0118916

Lind, B. L., Jessen, S. B., Lønstrup, M., Joséphine, C., Bonvento, G., and Lauritzen, M. (2018). Fast Ca^{2+} responses in astrocyte end-feet and neurovascular coupling in mice. *Glia* 66, 348–358. doi: 10.1002/glia.23246

Matrosov, V., Gordleeva, S., Boldyreva, N., Ben-Jacob, E., Kazantsev, V., and De Pittà, M. (2019). "Emergence of regular and complex calcium oscillations by inositol 1,4,5-trisphosphate signaling in astrocytes," in *Computational Glioscience*, eds M. De Pittà and H. Berry (Cham: Springer), 151–176.

Matsui, K., Jahr, C. E., and Rubio, M. E. (2005). High-concentration rapid transients of glutamate mediate neural-glial communication *via* ectopic release. *J. Neurosci.* 25, 7538–7547. doi: 10.1523/JNEUROSCI.1927-05.2005

Mergenthaler, K., Oschmann, F., and Obermayer, K. (2019). "Glutamate uptake by astrocytic transporters," in *Computational Glioscience* (Cham: Springer), 329–361.

Newman, E. A. (2004). A dialogue between glia and neurons in the retina: modulation of neuronal excitability. *Neuron Glia Biol.* 1, 245–252. doi: 10.1017/S1740925X0500013X

Pál, I., Kardos, J., Dobolyi, Á., and Héja, L. (2015). Appearance of fast astrocytic component in voltage-sensitive dye imaging of neural activity. *Mol. Brain* 8:35. doi: 10.1186/s13041-015-0127-9

Pál, I., Nyitrai, G., Kardos, J., and Héja, L. (2013). Neuronal and astroglial correlates underlying spatiotemporal intrinsic optical signal in the rat hippocampal slice. *PLoS One* 8:e57694. doi: 10.1371/journal.pone.0057694

Pallotto, M., Watkins, P. V., Fubara, B., Singer, J. H., and Briggman, K. L. (2015). Extracellular space preservation aids the connectomic analysis of neural circuits. *eLife* 4:e08206. doi: 10.7554/eLife.08206

Rusakov, D. A. (2015). Disentangling calcium-driven astrocyte physiology. *Nat. Rev. Neurosci.* 16, 226–233. doi: 10.1038/nrn3878

Rusakov, D. A., and Kullmann, D. M. (1998a). Extrasynaptic glutamate diffusion in the hippocampus: ultrastructural constraints, uptake and receptor activation. *J. Neurosci.* 18, 3158–3170. doi: 10.1523/JNEUROSCI.18-09-03158.1998

Rusakov, D. A., and Kullmann, D. M. (1998b). Geometric and viscous components of the tortuosity of the extracellular space in the brain. *Proc. Natl. Acad. Sci. U S A* 95, 8975–8980. doi: 10.1073/pnas.95.15.8975

Rusakov, D. A., Davies, H. A., Harrison, E., Diana, G., Richter-Levin, G., Bliss, T. V. P., et al. (1997). Ultrastructural synaptic correlates of spatial learning in rat hippocampus. *Neuroscience.* 80, 69–77. doi: 10.1016/s0306-4522(97)00125-5

Rusakov, D. A., Harrison, E., and Stewart, M. G. (1998). Synapses in hippocampus occupy only 1-2% of cell membranes and are spaced less than half-micron apart: a quantitative ultrastructural analysis with discussion of physiological implications. in *Neuropharmacology* 37, 513–521. doi: 10.1016/s0028-3908(98)00023-9

Rusakov, D. A., Kullmann, D. M., and Stewart, M. G. (1999). Hippocampal synapses: do they talk to their neighbours? *Trends Neurosci.* 22, 382–388. doi: 10.1016/s0166-2236(99)01425-3

Savtchenko, L. P., and Rusakov, D. A. (2007). The optimal height of the synaptic cleft. *Proc. Natl. Acad. Sci. U S A* 104, 1823–1828. doi: 10.1073/pnas.0606636104

Savtchenko, L. P., Bard, L., Jensen, T. P., Reynolds, J. P., Kraev, I., Medvedev, N., et al. (2018). Disentangling astroglial physiology with a realistic cell model in silico. *Nat. Commun.* 9:3554. doi: 10.1038/s41467-018-05896-w

Savtchenko, L., Megalogeni, M., Rusakov, D. A., Walker, M. C., and Pavlov, I. (2015). Synaptic GABA release prevents GABA transporter type-1 reversal during excessive network activity. *Nat. Commun.* 6:6597. doi: 10.1038/ncomms7597

Semyanov, A., Henneberger, C., and Agarwal, A. (2020). Making sense of astrocytic calcium signals—from acquisition to interpretation. *Nat. Rev. Neurosci.* 21, 551–564. doi: 10.1038/s41583-020-0361-8

Somogyi, P., Eshhar, N., Teichberg, V. I., and Roberts, J. D. B. (1990). Subcellular localization of a putative kainate receptor in Bergmann glial cells using a monoclonal antibody in the chick and fish cerebellar cortex. *Neuroscience* 35, 9–30. doi: 10.1016/0306-4522(90)90116-l

Stobart, J. L., Ferrari, K. D., Barrett, M. J. P., Glück, C., Stobart, M. J., Zuend, M., et al. (2018). Cortical circuit activity evokes rapid astrocyte calcium signals on a similar timescale to neurons. *Neuron* 98, e4726–e4735. doi: 10.1016/j.neuron.2018.03.050

Szabó, Z., Héja, L., Szalay, G., Kékesi, O., Füredi, A., Szebényi, K., et al. (2017). Extensive astrocyte synchronization advances neuronal coupling in slow wave activity *in vivo*. *Sci. Rep.* 7:6018. doi: 10.1007/s11356-020-09610-6

Harreveld, A. V., and Fifkova, E. (1975). Rapid freezing of deep cerebral structures for electron microscopy. *Anat. Rec.* 182, 377–385. doi: 10.1002/ar.1091820311

Van Harreveld, A., and Khattab, F. I. (1968). Chloride movements during perfusion fixation with glutaraldehyde. *Anat. Rec.* 162, 467–477. doi: 10.1002/ar.1091620408

Ventura, R., and Harris, K. M. (1999). Three-dimensional relationships between hippocampal synapses and astrocytes. *J. Neurosci.* 19, 6897–6906. doi: 10.1523/JNEUROSCI.19-16-06897.1999

Wu, Y.-W., Gordleeva, S., Tang, X., Shih, P.-Y., Dembitskaya, Y., and Semyanov, A. (2019). Morphological profile determines the frequency of spontaneous calcium events in astrocytic processes. *Glia.* 67, 246–262. doi: 10.1002/glia.23537

Zhang, Y., Sloan, S. A., Clarke, L. E., Caneda, C., Plaza, C. A., Blumenthal, P. D., et al. (2016). Purification and characterization of progenitor and mature human astrocytes reveals transcriptional and functional differences with mouse. *Neuron* 89, 37–53. doi: 10.1016/j.neuron.2015.11.013

Ziemens, D., Oschmann, F., Gerkau, N. J., and Rose, C. R. (2019). Heterogeneity of activity-induced sodium transients between astrocytes of the mouse hippocampus and neocortex: mechanisms and consequences. *J. Neurosci.* 39, 2620–2634. doi: 10.1523/JNEUROSCI.2029-18.2019